ACS APPLIED MATERIALS & INTERFACES

Research Article

www.acsami.org

Superhydrophobic Nanocomposite Surface Topography and Ice Adhesion

Alexander Davis,*[,†,‡] Yong Han Yeong,[†] Adam Steele,[†] Ilker S. Bayer,*[,†,‡] and Eric Loth[†]

[†]Department of Mechanical and Aerospace Engineering, University of Virginia, Charlottesville, Virginia 22904, United States
[‡]Smart Materials, Nanophysics, Istituto Italiano di Tecnologia, Genoa 16163, Italy

Supporting Information

ABSTRACT: A method to reduce the surface roughness of a spray-casted polyurethane/silica/fluoroacrylic superhydrophobic nanocomposite coating was demonstrated. By changing the main slurry carrier fluid, fluoropolymer medium, surface pretreatment, and spray parameters, we achieved arithmetic surface roughness values of 8.7, 2.7, and 1.6 μm on three test surfaces. The three surfaces displayed superhydrophobic performance with modest variations in skewness and kurtosis. The arithmetic roughness level of 1.6 μm is the smoothest superhydrophobic surface yet produced with these spray-based techniques. These three nanocomposite surfaces, along with a polished aluminum surface, were impacted with a supercooled water spray in icing conditions, and after ice accretion occurred, each was subjected to a pressurized tensile test to measure ice-adhesion. All three superhydrophobic surfaces showed lower ice adhesion than that of the polished aluminum surface. Interestingly, the intermediate roughness surface yielded the best performance, which suggests that high kurtosis and shorter autocorrelation lengths improve performance. The most ice-phobic nanocomposite showed a 60% reduction in ice-adhesion strength when compared to polished aluminum.

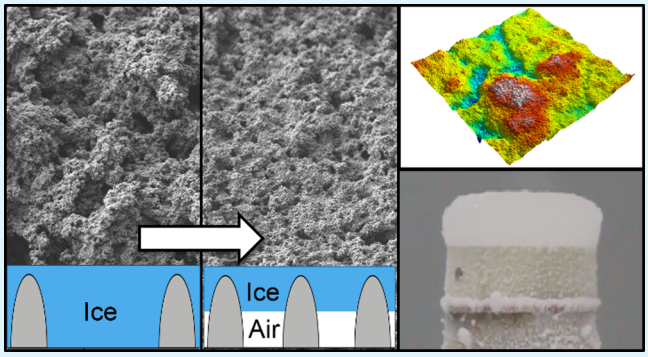

KEYWORDS: *anti-icing, superhydrophobic, nanocomposite, spray-coating, roughness, polyurethane, silicon dioxide*

1. INTRODUCTION

Superhydrophobic coatings have drawn great interest as an energy independent technique to delay ice accretion and lower ice adhesion on power lines, aircraft, and wind turbines. Meuler et al.[1] found that the introduction of surface texture was able to decrease ice adhesion strength to less than what was achievable just through chemical modification. Coatings that can be applied through one-step spray casting are particularly desirable because of their relatively low cost and ease of application. However, such surfaces are typically characterized with relatively high levels of arithmetic roughness.

Minimizing arithmetic roughness can be important for aerodynamic surfaces (such as on aircraft or wind turbines) because higher roughness detrimentally increases the skin friction coefficient for a turbulent boundary layer and causes a laminar boundary to undergo transition more quickly.[2] In both cases, this increases the drag on surfaces, and thus, adding surface features to attain superhydrophobicity on aerodynamic surfaces represents a potential negative side effect with respect to skin friction drag. Therefore, it is aerodynamically desirable to create a surface with low roughness while maintaining superhydrophobicity.

Another reason to reduce roughness stems from resistance to ice attachment. Large-scale roughness on a superhydrophobic surface can allow the surface asperities to be infiltrated with impacting water droplets, causing a transition from the nonwetting Cassie state to the wetting Wenzel state, known herein as saturation. Ice that has saturated the surface asperities can create a tight bond with the surface, increasing the strength of ice adhesion. For example, the delay time of ice accretion onto a superhydrophobic surface with nanoscale roughness was observed to be higher than one with microscale roughness when tested in an icing wind tunnel.[3] Another study found that ice adhesion strength decreased as the surface area of textured PDMS decreased.[4]

Although work has been done in the past to control the roughness features of surfaces created through micromolded polymers,[5] plasma treatment,[6,7] electrodeposition,[8] and electrospinning,[9] there has not been, to the authors' knowledge, a similarly detailed study for a spray casted superhydrophobic coating. Instead, the focus for spray casted surfaces has been on other performance aspects (e.g., coating adhesion, omniphobicity, durability, etc.), and typical nanocomposite surfaces have had arithmetic roughness on the order of 10 μm.[10,11] As such, reducing roughness levels to values on the order of 1−2 μm while maintaining superhydrophobicity has been identified as an important objective for spray-cast coatings.[12]

Received: March 18, 2014
Accepted: May 29, 2014
Published: May 29, 2014

There were two key objectives to this study: The first objective was to refine the process to create smoother spray-casted polyurethane/fluoropolymer/silica superhydrophobic coatings by removing finish defects and changing the self-assembly process. The main precursor slurry solvent, fluoropolymer medium, surface pretreatment, and spray parameters were varied to produce nanocomposite coatings, and antiwetting performance and surface topography were measured. The second objective was to investigate the ability of these nanocomposite surface to reduce ice adhesion in an icing condition similar to that observed in aerospace applications. Therefore, three nanocomposite superhydrophobic surfaces with different degrees of roughness, along with a baseline polished aluminum sample, were exposed to a spray of supercooled water droplets in a refrigerated chamber. Ice was allowed to accrete on each surface, and the ice adhesion strength was measured to determine the efficacy of introducing superhydrophobicity and to note performance changes that may be due to varying roughness.

2. METHODS

2.1. Surface Preparation. After several trials, we developed three different superhydrophobic coating formulations that produced finished surfaces with arithmetic mean surface roughness values of 8.7 μm (SH-8), 2.7 μm (SH-3), and 1.6 μm (SH-1). All samples were sprayed with the same spray casting process described by Yeong,[13] with aluminum substrates lying on a motorized platform traversing longitudinally and laterally while the spray gun was held stationary. A photo of the setup is shown in Figure 1. The formulations, surface preparation, and spray parameters for each surface are listed in Table 1. SH-8 was the initial surface formulation and consisted of a single-stage two-component urethane paint (Dupont) mixed in a vial with silica nanopowder (Sigma-Aldrich), acetone, and waterborne perfluoroalkyl methacrylic copolymer (PMC, Dupont, ~80 wt % H_2O). This emulsion was vortex mixed for several minutes and then sprayed onto aluminum (320-grit sanded to promote mechanical adhesion between coating and substrate) using a conventional siphon atomizing spray nozzle (1/4JCO series, Spraying Systems Co., Wheaton, IL) with an air pressure of ~200 kPa and spray distance of 9 cm. The coating was then immediately heat cured at 100 °C for 6 h.

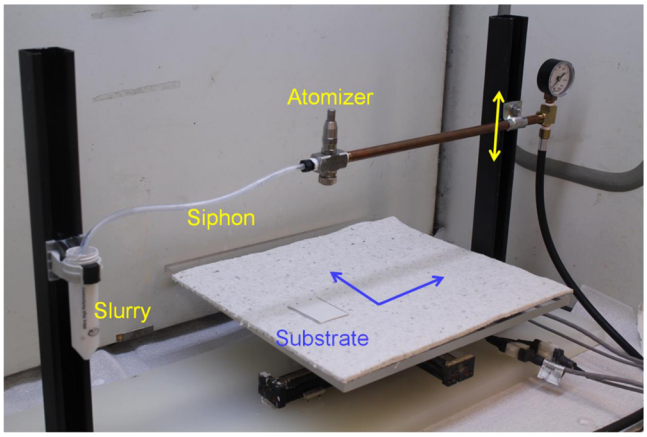

Figure 1. Photo of the automated spray-coating setup. The nanocomposite formulation is siphoned to the atomizer, while the substrate translates in a raster pattern below.

The formulation of SH-3 employed changes that successfully reduced the surface roughness. The same urethane paint, silica nanopowder, and waterborne PMC were vortex mixed. Instead of dispersing in acetone, a commercial urethane reducer (Dupont) consisting of a 90:10 (v/v) parachlorobenzotrifluoride(PCBTF)/acetone mixture, was used as the solvent. SH-3 was vortex mixed and spray casted with the same air pressure as SH-8 and was immediately heat cured. However, the spray distance was increased to 11 cm for SH-3. This change was made because at closer spray distances, atomizing air tended to deform the still-wet film.

Table 1. Surface Formulations and Their Preparation Procedures

	SH-1	SH-3	SH-8
PU wt %	25	24	24
PCBTF	33	29	0
acetone	33	29	58
water	0	12	12
PMC	5	3	3
silica	3	3	3
mixing	sonication	vortex	vortex
surface cleaning	yes	no	no
spray distance	15 cm	11 cm	9 cm
air pressure	340 kPa	200 kPa	200 kPa

The most successful formulation to reduce surface roughness was SH-1. In this case, urethane paint and silica nanopowder were dispersed in the previously mentioned urethane reducer. In a separate vial, equal volumes of trifluoroacetic acid (Fisher) and waterborne PMC were mixed, causing fluoropolymer to come out of solution. While the as-received waterborne PMC solution had a slightly hazy orange color, when out of solution, the orange color of the polymer and the white color of the surfactants that stabilize the as-received latex became clearly visible. The solid fluoropolymer was then redispersed in urethane reducer and vortex mixed into the PU/silica/reducer emulsion. The entire mixture was sonicated at 35% amplitude and a frequency of 20 kHz for 2 min with an ultrasonicator (Model VC750, Sonics & Materials, Inc., Newtown, CT). Viscosity was measured to be 15 s using a Zahn #2 cup (Gardco EZ Cup). The stability of SH-1 was also better than the other two formulations; the surfactants present in the as-received fluoropolymer were not compatible with acetone, so agitation was required to keep SH-8 and SH-3 from separating into two phases within a few seconds. Without surfactants present, SH-1 remained stable without agitation.

In addition to being sanded, the aluminum substrate was washed with isopropyl alcohol to remove any contaminants such as wax or grease from the surface. The mixture was then sprayed using the same nozzle as mentioned above except at an air pressure of 340 kPa and spray distance of 15 cm. This larger distance and higher pressure allowed for smaller drops and more evaporation.[14] SH-1, unlike SH-8 and SH-3, was allowed to flash off (all of the solvent left on the substrate after spray-coating evaporated after a period of 40 min) before being heat cured.

2.2. Surface Wettability and Topography Characterization. To characterize surface wettability, static contact angle and contact angle hysteresis were measured at five different locations on each surface using a ramé-hart Model 290 goniometer. For superhydrophobic surfaces, contact angle hysteresis was measured using the tilting plate method with a 10 μL droplet. The sessile drop method was used to measure contact angle hysteresis for the polished aluminum surface because droplets were not able to slide off the surface when tilted (i.e., "pinned" state). In this method, a 2 μL droplet was initially placed on the polished aluminum surface. Water was added to the sessile droplet in increments of 0.25 μL until the three phase contact line expanded, at which point the advancing contact angle was recorded. Water was then subtracted from the droplet again in 0.25 μL increments until the contact line retracted, and the receding contact angle was recorded.

For surface morphology visualization, samples were coated with a 12 nm thick layer of Au/Pd to reduce surface charging, and scanning electron microscope (SEM) images were taken of superhydrophobic samples using a JEOL 6700F FESEM. Samples were tilted at 30° to more greatly bring out differences in morphology. Energy dispersive X-

Scheme 1. Schematic Illustration of the Ice Adhesion Experiment[a]

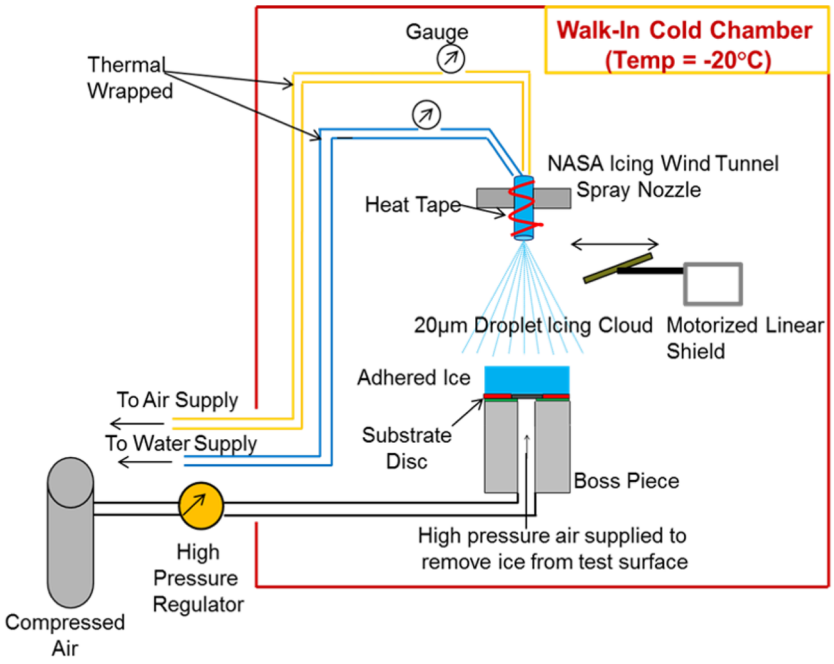

[a]Ice is accreted onto surfaces by spraying supercooled water droplets, which freeze on impact. Air is then pressurized in a defect between the tested surface and the ice until the interface is fractured.

ray spectroscopy (EDS) measurements were made using a PGT IMIX-SPIRIT detector. Confocal laser scanning microscope scans (CLSM) of the surfaces were done using a Zeiss LSM 510 at five different locations on each surface. After initial scans, a robust Gaussian filter with a 4 μm cutoff was applied to the surface topography using the MountainsMap topography software (Digital Surf). Surface features were then calculated from the filtered topography.

2.3. Ice Adhesion Test. An experiment was designed to measure the ice adhesion strength on the superhydrophobic surfaces. The ice was accreted by exposing the surfaces to supercooled water droplets in a freezing environment where the droplets impinged upon the surfaces and nucleated to form a layer of ice. This mechanism of ice accretion is typically observed in aircraft and wind turbine applications.

The basic components of the icing experiment is shown in Scheme 1. The coatings were applied on an aluminum disc substrate, which was attached to an aluminum cylinder boss piece and placed in a walk-in cold chamber (Leer) with an access hole. The attached substrate and boss piece were then positioned under an air-atomizing nozzle. This nozzle (Mod-1) was acquired from the icing branch at the NASA Glenn Research Facility and was specifically designed to produce a spray consisting of 20 μm water droplets. Deionized water (separately cooled to 5 °C) and air for the Mod-1 nozzle was supplied from a water pump (Cole Parmer) and air compressor (Craftsman) installed outside of the cold chamber and connected to the nozzle via thermally wrapped hoses through the chamber access hole. Once the cold chamber was cooled to −20 °C, the spray was initiated at water and air pressures of 450 and 140 kPa, respectively, to accrete a layer of ice with a thickness of 10 mm on the disc substrate. The optimal distance between the spray nozzle and the disc substrate was found to be 78 cm. At this distance, water droplets were supercooled before coming in contact with the coating. This created an ice structure that coherently accreted on top of the disc substrates. As shown in Figure S1 in the Supporting Information, if the distance was too close, droplets were not supercooled and did not freeze on impact, resulting in a "flowing" ice condition. If the distance was too far, the droplets froze during flight, resulting in an accretion of snowflakes on the substrate.

After the accretion was completed, pressurized air was increasingly supplied at a rate of approximately 14 kPa/s from a compressed gas tank located outside of the freezer to the boss piece and through the hole in the substrate disc until the accreted ice was fractured and removed from the surface. This pressure was recorded via a pressure transducer as the ice fracture pressure of the substrate. The ice adhesion test described here was repeated three times for each coating, with each surface reused for successive tests. After each icing test, the coatings were returned to room temperature overnight, maintaining their original superhydrophobic state.

3. RESULTS

3.1. Surface Topography. Topography for irregular surfaces can be described by characteristics associated with the largest perturbations, including roughness, skewness, kurtosis, slopes, and lateral lengths, as well as characteristics associated with the hierarchal nature, including fractal dimension, spectral range, and so on. Herein, the focus is on the first set of characteristics as these are most important to characterize skin friction drag on aerodynamic surfaces and have been most commonly correlated to ice adhesion performance. In particular, the most common surface property is the arithmetic mean surface roughness, S_a, defined as

$$S_a = \frac{1}{N \times M} \sum_{j=1}^{N} \sum_{i=1}^{M} |z_{i,j}| \quad (1)$$

In this expression, z is the vertical distance perpendicular and relative to the mean plane of the surface, while M and N are the number of points sampled in the lateral x and y directions, respectively.

Representative CLSM scans of the superhydrophobic samples are shown in Figure 2. The surface height distribution of SH-8 is shown in Figure 2a and has significant peaks and valleys. The mean roughness in this case is 8.7 mm, which is typical of spray-casting nanocomposite surfaces, as discussed in the Introduction. This formulation used a solvent of pure acetone. With a very high vapor pressure (184 mmHg at 20 °C), the acetone evaporated quickly when atomized while

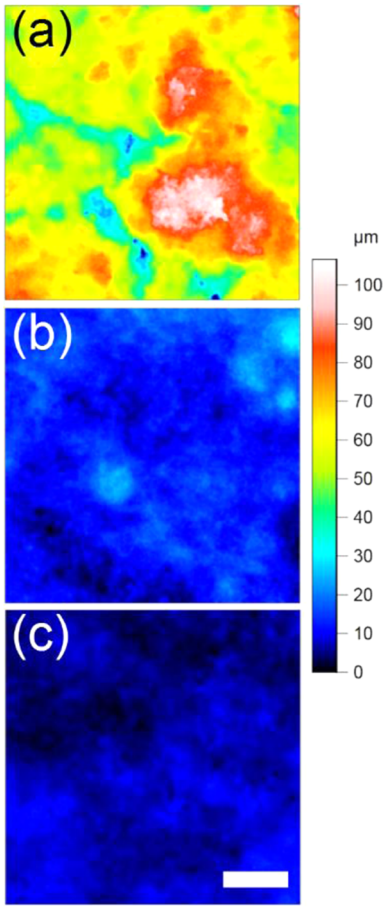

Figure 2. Confocal microscopy scans of (a) SH-8, (b) SH-3, and (c) SH-1 superhydrophobic coatings. Colors indicate height from a minimum location. Scale bar = 100 μm. On the basis of the height fluctuations from the mean, surface roughness (S_a) greatly decreased, as formulation changed from 8.7 μm for SH-8 to 1.6 μm for SH-1.

creating SH-8, resulting in a rough surface without much leveling. Significant cracking in the film was also apparent, as seen in Figure 3a. Not only does this contribute to surface roughness and integrity of the film, cracks in the coating provide surface area to which accreted ice adheres. It is even possible for a crack in the coating to expose bare substrate. For SH-3, the solvent was changed to a commercial urethane reducer that included PCBTF (vapor pressure = 5 mmHg at 20 °C), and much less carrier liquid evaporated during spray casting. This resulted in a more level surface and a roughness of 2.7 μm. Also noticeable was the decrease in cracking in the film, as seen in Figure 3b.

As noted in the Introduction, it was desired to reduce the roughness even further. For SH-1, the lower surface tension of the PMC/reducer solution (25 mN/m) than the as-received waterborne PMC solution (72 mN/m) enabled better substrate wetting and a more unified film, as cracking in the film decreased. Washing the aluminum substrate with isopropyl alcohol before spraying also eliminated "craters" on the surface that are caused by contaminants. In addition, allowing the sprayed surface to flash off before heat curing allowed the surface to level as much as possible, and S_a was reduced to 1.6 μm. The morphology of SH-1, seen in Figure 3c, shows a much more uniform and homogeneous film, brought about by using a carrier fluid that allowed for leveling the coating and wetting the substrate before evaporation. The arithmetic roughness level of 1.6 μm is the smoothest superhydrophobic surface yet produced with these spray-based nanocomposite techniques.

The distribution of surface heights from the mean plane (e.g., a height of 5 μm corresponds to 5 μm above mean plane, a height of −5 μm corresponds to 5 μm below the mean plane) was calculated, and the probability density function of these heights is shown in Figure 4. It is clear that as S_a decreases, the distribution becomes more tightly bound around the mean plane. Skewness is the nondimensional measure of asymmetry of surface heights around the mean plane and is defined as

$$S_{sk} = \frac{1}{(N \times M)S_q^3} \sum_{j=1}^{N} \sum_{i=1}^{M} z_{i,j}^{\ 3} \qquad (2)$$

where

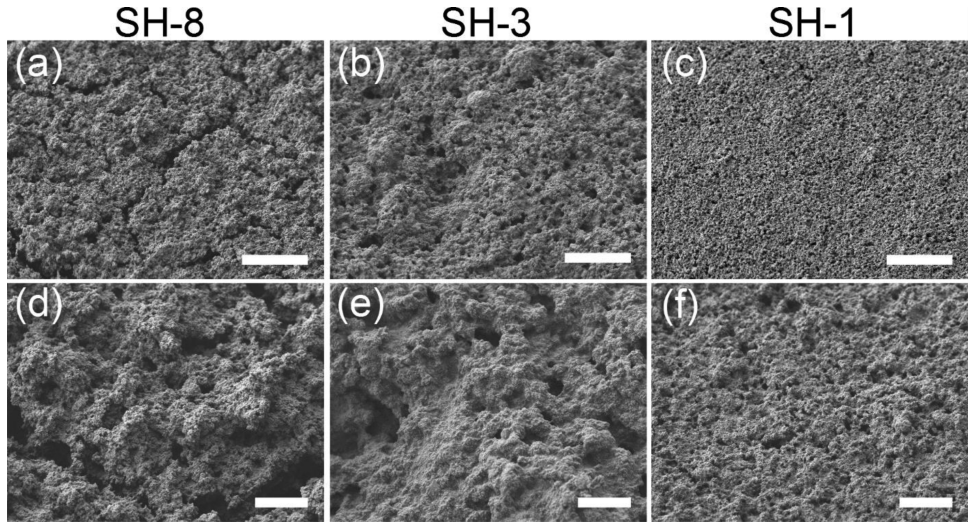

Figure 3. SEM images of (a and d) SH-8, (b and e) SH-3, and (c and f) SH-1. Panels d–f are higher magnification images. A reduction in surface cracking and increase in general homogeneity were seen as a result of changing formulation and spray parameters. Top row: scale bar = 100 μm. Bottom row: scale bar = 20 μm.

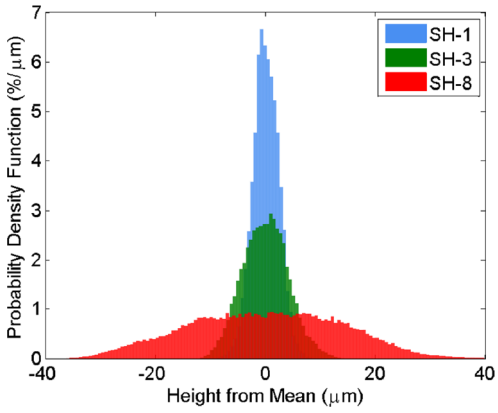

Figure 4. Probability density function of surface heights from the mean plane. The widespread of SH-8 corresponds to relatively large surface features and high S_a, whereas the narrow spread of SH-1 shows lower S_a.

$$S_q = \sqrt{\frac{1}{N \times M} \sum_{j=1}^{N} \sum_{i=1}^{M} z_{i,j}^{\ 2}} \tag{3}$$

For example, a surface with positive skewness would be composed of "hills", while negative skewness corresponds to "valleys". Kurtosis is the nondimensional measure of peakedness of surface heights, and is defined as

$$S_{kur} = \frac{1}{(N \times M) S_q^4} \sum_{j=1}^{N} \sum_{i=1}^{M} z_{i,j}^{\ 4} \tag{4}$$

A surface with high kurtosis would exhibit spiky features, while a surface with low kurtosis would show more blunt topography, with the kurtosis of a Gaussian distribution equal to 3. Kulinich et al.[15] found that spin-coated surfaces with high skewness and high kurtosis (values of 5.02 and 25.13, respectively), corresponding to a morphology akin to spiky mountains, were conducive to high contact angle and low hysteresis, whereas spray-coated surfaces with negative skewness and low kurtosis (values of −1.27 and 7.36, respectively), with morphology similar to rounded valleys, displayed high contact angle but high hysteresis.

The above parameters give information about the height and shape of surface features (i.e., peaks and valleys). To quantify the lateral spatial variation of peaks and valleys, one may employ the autocorrelation function (G) which is defined as[16]

$$G(\tau_x, \tau_y) = \frac{1}{S_q} \iint_s z(x, y)\, z(x + \tau_x, y + \tau_y)\, dx\, dy \tag{5}$$

where τ_x and τ_y are lateral incremental distances in the x and y directions. This integral can be discretized as

$$G(\tau_x, \tau_y) = \frac{1}{(N \times M) S_q} \sum_{j=1}^{N} \sum_{i=1}^{M} z_{i,j} z_{i+m,j+n} \tag{6}$$

where $m = \tau_x/\Delta x$ and $n = \tau_y/\Delta y$. For an irregular random surface, this correlation approaches unity as these distances approach 0 and approaches 0 as these distances approach infinity. The variation rate between these two extremes can generally be assumed to be an exponential between 0 and 1. One may define an autocorrelation length S_{al} as the minimum lateral distance

$$S_{al} = \sqrt{(\tau_x^{\ 2} + \tau_y^{\ 2})} \tag{7}$$

such that $G(\tau_x, \tau_y)$ decays to a value of 0.2. In practice, S_{al} is used as a measure of the distance required to traverse from one point on a surface to an unrelated point (e.g., one peak to another) with a low S_{al} indicating a surface with less space between peaks.[17]

Surface roughness, skewness, kurtosis, and autocorrelation length of each tested surface are reported in Table 2. Polished aluminum exhibited the smallest S_a (0.45 μm), as expected, and a kurtosis of 3.1, nearly equal to that of a Gaussian distribution. As discussed above, the nanocomposite surfaces had roughness values that varied from 8.7 to 1.6 μm among the three surfaces. While the roughness decreased, the values of kurtosis and skewness varied little for the present surfaces (as compared to the large variations reported in the literature for other irregular superhydrophobic surfaces). This indicates that feature shapes of the present surfaces were approximately maintained as the height was reduced. Furthermore, surfaces features were nearly symmetric (S_{sk} values close to 0.0) and nearly Gaussian (S_{kur} values close to 3.0). However, some trends were observed for the superhydrophobic surfaces. In particular, SH-1 had a lower S_{kur} and a higher S_{sk} than SH-3 and SH-8. The fast evaporation of solvent during spraying and low wetting of the substrate that caused increased roughness might have produced surfaces with sharper peaks in the dried coating.

Table 2. Surface Texture Measurements of Polished Aluminum and Superhydrophobic Coatings[a]

surface	S_a (μm)	S_{sk}	S_{kur}	S_{al} (μm)
polished Al	0.45	−0.17	3.1	145
SH-1	1.6	0.28	3.6	57
SH-3	2.7	0.19	4.0	39
SH-8	8.7	0.19	4.2	70

[a]Arithmetic roughness (S_a), skewness (S_{sk}), and kurtosis (S_{kur}) are height parameters that indicate the shape of surface features. Autocorrelation length (S_{al}) is a spatial parameter that indicates spacing of surface features. S_a was successfully decreased due to changes in nanocomposite slurry formulation and spray procedures. Surface topography measurements were not greatly affected by applying the robust Gaussian filter, with measurements before and after shown in Table S1 in the Supporting Information.

In contrast to the skewness and kurtosis, a larger variation in S_{al} was observed among the different samples. As a smooth, homogeneous surface, polished aluminum showed the highest S_{al} (145 μm), indicating relatively long wavelengths for its surface variations. In contrast, all the superhydrophobic surfaces had a much smaller lateral length scale; SH-3 had the lowest length-scale value (39 μm), indicating its features are the most closely spaced.

3.2. Surface Wettability. Wetting performance of all surfaces are given in Table 3. The aluminum surface was weakly hydrophilic with static and advancing angles close to but below 90°. This surface had a relatively high hysteresis and droplets were pinned to the surface regardless of the tilt angle. All SH surfaces yielded static and advancing angles between 158° and 161°, showing remarkable consistency. All SH surfaces showed a roll-off angle (ROA) less than 6°. The SH-8 surface gave the best performance with hysteresis and ROA values of 7° and 2°, respectively; while SH-3 yielded the highest hysteresis and ROA values (15° and 5°, respectively).

Table 3. Wetting Characteristics of Tested Surfaces[a]

surface	contact angle				ROA
	static	advancing	receding	hysteresis	
polished Al	77°	87°	20°	57°	pinned
SH-1	160°	161°	151°	10°	4°
SH-3	158°	159°	144°	15°	5°
SH-8	159°	159°	152°	7°	2°

[a]Wettability was largely maintained even though average roughness was decreased from 8.7 μm for SH-8 to 1.6 μm for SH-1.

3.3. Chemical Topology. In addition to geometric features, the chemical topography can be important for a superhydrophobic surface. SEM images of SH-1, shown in Figure 5, reveal the two particles present in the coating. The larger particles are titanium dioxide (TiO_2) pigments that are present in the as-received urethane paint. The higher atomic number of titanium causes them to appear brighter than the surrounding material when a backscattered detector is used, as shown in Figure 5a. These pigments give the coating a white hue and serve as UV protection. The smaller particles are the dispersed silica nanoparticles. TiO_2 pigments were measured to have diameters in the range of 200−300 nm, while SiO_2 particles had diameters of <100 nm. The particles were identified by their size and by EDS, shown in Figure 5c,d. When focused on a group of presumed TiO_2 pigments, EDS revealed large peaks at ∼4.5 and 4.9 keV, corresponding to the K_α and K_β absorption energies of titanium. Similarly, a peak at 1.7 keV appeared when the detector focused on suspected SiO_2 particles, corresponding to silicon's K_α absorption energy. Three scales of roughness (and chemistry) are then found in the coating: (1) microscale roughness of the film itself, as discussed in section 3.2, (2) nanoscale roughness of the TiO_2 pigments, and (3) nanoscale roughness of the SiO_2 particles.

3.4. Ice Adhesion Performance. Images of ice accreting on a surface during an ice adhesion test are shown in Figure 6. Upon being exposed to the supercooled spray, ice continually formed on the surface. After 135 s of being exposed to the supercooled spray, approximately 10 mm of ice was accreted on the sample surface, as shown in Figure 6c. Finally, pressurized air was able to fracture the ice−solid interface, causing the accreted ice to be separated from the surface.

The average pressures required to fracture the ice−solid interface are shown for each tested surface in Figure 7, with error bars extending to the minimum and maximum fracture pressure observed. Polished aluminum exhibited an average fracture pressure of 1670 kPa, the highest pressure required for all surfaces tested. An average fracture pressure of 1430 kPa was required for SH-8, the roughest superhydrophobic surface. SH-1 displayed an average fracture pressure of 1010 kPa, while SH-3 displayed the most ice-phobicity with a fracture pressure of 680 kPa, a reduction of 60% compared to the baseline polished aluminum. The fact that the adhesion was not reduced further may be related to chemical topography. In particular, because the TiO_2 and SiO_2 particles are hydrophilic, they may act as nucleation sites for ice accretion at specific sites and promote local fractures of ice during the ice-adhesion tests.

The effect of repeated icing/deicing cycling on maintaining the efficacy of anti-icing coatings has become an important part of research.[18,19] This can be related to the fact that during ice fracture, part of the coating can fracture or chip away. This is strongly related to how good the adhesion is between the coating and the substrate. Interestingly, fracture pressure was not greatly affected by icing/deicing cycles for the current coatings. In particular, during the ice fracture tests that were

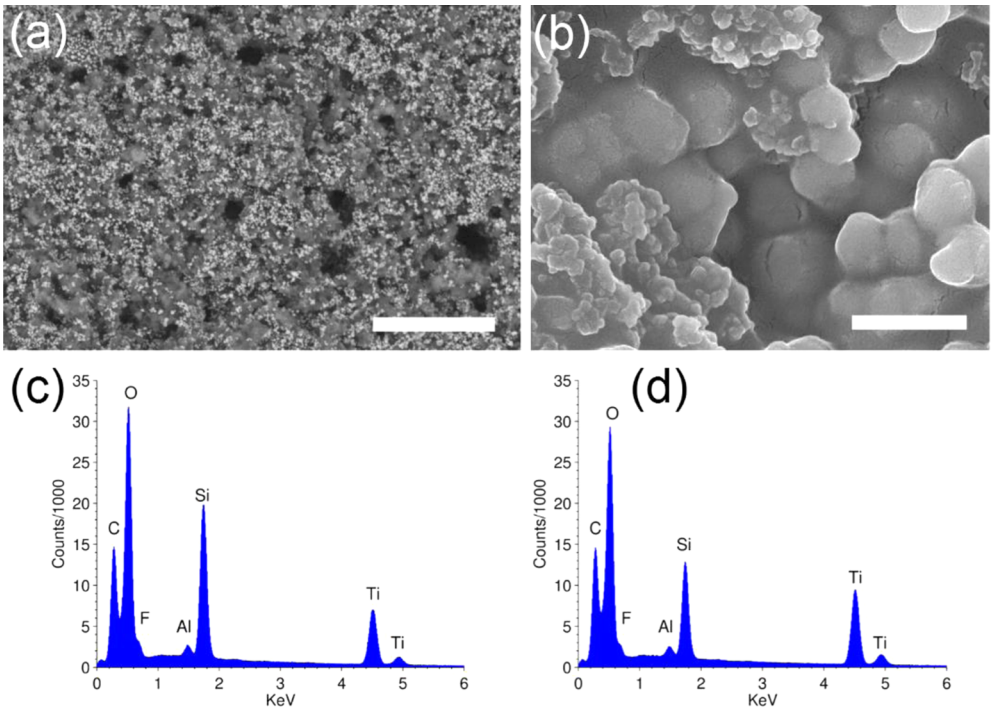

Figure 5. (a) Backscattered SEM of SH-1 surface, with heavier TiO_2 pigments appearing brighter than the polyurethane matrix and SiO_2 particles. Scale bar = 10 μm. (b) High magnification secondary electron SEM with smaller SiO_2 particles also visible. Scale bar = 500 nm. (c) EDS spectrum when focused on SiO_2 particles. (d) EDS spectrum when focused on TiO_2 pigments.

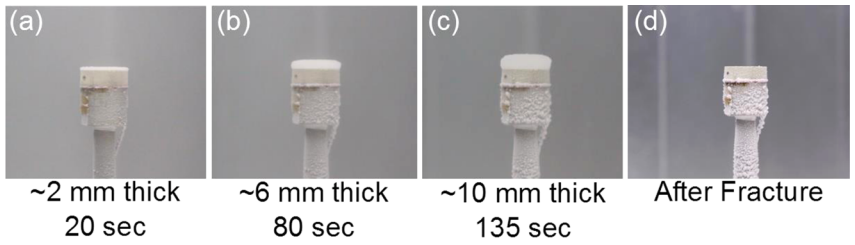

Figure 6. Time evolution of icing experiment. (a–c) Ice steadily accumulates until a thickness of 10 mm is reached. (d) Air is pressurized until a fracture forms between the accumulated ice and the ice-phobic coating.

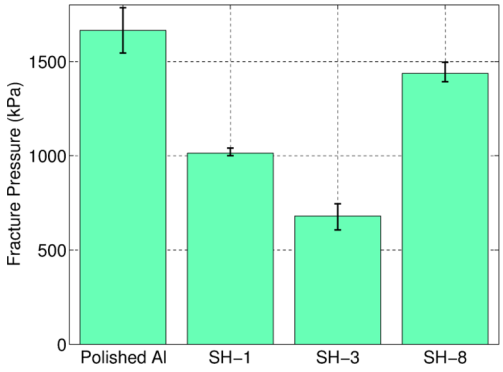

Figure 7. Average ice fracture pressures of all surfaces tested. Error bars indicate the minimum and maximum fracture pressure of the three repetitions for each surface. An average of 1670 kPa of pressurized air was required to fracture the interface between ice and the baseline polished aluminum. All superhydrophobic nanocomposites showed a lower fracture pressure; SH-3 required only 680 kPa.

repeated three times, there was no degradation in the superhydrophobicity of surfaces once they dried under room conditions. In fact, the variation in fracture pressure for each of the superhydrophobic surfaces was less than that of the polished aluminum, indicating that their variation was less than the uncertainty of the icing test itself for the limited number of cycles employed herein (three). This strong performance may be related to the very high adhesion between the coating and the substrate due to the integration of polyurethane in the coating.[10]

On the basis of previous studies, it was hypothesized that reducing S_a and increasing S_{sk} would correspond to lower fracture pressure if wetting characteristics were nearly equal. This result is consistent when comparing SH-1 with SH-8. However, despite having an intermediate S_a (Table 2) and the highest roll-off angle (Table 3), SH-3 yielded the lowest ice adhesion. In fact, even with lower roughness, SH-1 showed lower contact angle hysteresis than SH-3. As a result, one should also consider the influence of kurtosis. In general, lower values of kurtosis (S_{kur}) have been shown in previous studies to increase ice adhesion. For example, etched aluminum that had been coated with stearic acid was subjected to multiple icing/deicing cycles, resulting in a decrease in S_{kur} and an increase in shear stress (required for ice removal) from 50 to 200 kPa.[20] In another case, the freezing time of water droplets on CeO_2 doped silicone rubber (SR) was found to be longer than the freezing time of water droplets on TiO_2 doped SR, owing to a higher S_{kur} even though S_{sk} was lower.[21] These previous studies indicate that a reduction in ice adhesion may be expected for high S_{kur} surfaces and is attributed to the spiky peaks having less liquid–solid contact area when wetted in the Cassie–Baxter mode than rounded peaks, and thus less ice–solid contact area. This proposed correlation of high kurtosis with low ice-adhesion could then explain the difference between SH-3 and SH-1, but it appears to be secondary with respect to roughness and skewness when comparing SH-3 and SH-8. Therefore, it is difficult to make a direct conclusion regarding the influence of S_a, S_{sk}, and S_{kur}.

Yet another parameter that may be considered is that of autocorrelation length. In particular, it can be seen that comparing the S_{al} values in Table 2 with the ice fracture pressures in Figure 7, there is a consistent decrease in fracture pressure as S_{al} decreases across all four samples. This correlation may be attributed to the increased likelihood that the small droplets (about 20 μm in diameter) are less likely to saturate and become lodged in surface asperities if the features are closer together.[22] If supercooled droplets are only allowed to freeze at the top of surface asperities, as opposed to inside them, less room is available for ice–solid contact, and ice adhesion will be lowered. As the spatial features are farther apart (high S_{al}), a transition to the Wenzel wetting state is more likely, and more area is available for ice–solid contact. While this is a plausible explanation, given the small data set considered herein (four samples), it is difficult to determine which surface features are most important for spray-cast nanocomposite coatings for aerospace icing conditions. In particular, possible surface features that may be important to reduce ice adhesion include reduced arithmetic roughness, reduced polymer cracking, increased skewness, increased kurtosis, and reduced autocorrelation length. Further experiments including a larger number of sample substrates and coatings and a wide variation of surface parameters (potentially extending to hierarchal characteristics) are important to help determine the appropriate functional relationships. However, it can be concluded that the present superhydrophobic surfaces demonstrated reduced ice adhesion in aerospace icing conditions, while this study also demonstrated formulations and spray-casting methods to reduced coating roughness, a characteristic that is critical to improved aerodynamic performance.

4. CONCLUSIONS

In this experimental study, the surface roughness of a spray casted superhydrophobic coating was systematically reduced. The initial coating (SH-8), using acetone and water as cosolvents and no surface cleaning, produced an S_a of 8.7 μm and significant film heterogeneity. SH-3 achieved a decrease in S_a to 2.7 μm, and an improvement in film quality was achieved by changing the main solvent to a commercial urethane reducer that included a slower evaporating solvent. For SH-1, water was replaced as the PMC medium by the urethane reducer, giving a further decrease in S_a to 1.6 μm. All three surfaces showed a similar high level of water repellency and all three surfaces

showed reduced ice adhesion levels as compared to an aluminum surface. In addition, these levels were maintained over three cycles for all coatings, indicating no degradation in performance during repeated icing and deicing. Finally, reduced ice adhesion showed correlation with increased hydrophobicity, reduced roughness, increased skewness and kurtosis, and reduced autocorrelation length. However, further experiments with a larger number of samples and a wide variation of parameters are important to isolate the individual influence of these surface characteristics with respect to aerospace ice adhesion.

■ ASSOCIATED CONTENT

Supporting Information

Experimental details of optimizing the spray distance for the ice adhesion test and the effect of the robust Gaussian filter on surface topography data. This material is available free of charge via the Internet at http://pubs.acs.org.

■ AUTHOR INFORMATION

Corresponding Authors

*E-mail: alexander.davis@iit.it.
*E-mail: ilker.bayer@iit.it

Notes

The authors declare no competing financial interest.

■ ACKNOWLEDGMENTS

This work was performed under a contract for Rolls-Royce North America through the Commonwealth Center for Advanced Propulsion with supervision by Dr. Jack Sokhey.

■ REFERENCES

(1) Meuler, A. J.; Smith, J. D.; Varanasi, K. K.; Mabry, J. M.; McKinley, G. H.; Cohen, R. E. Relationships between Water Wettability and Ice Adhesion. *ACS Appl. Mater. Interfaces* **2010**, *2*, 3100−3110.

(2) White, F. *Fluid Mechanics*, 7th ed.; McGraw-Hill: New York, 2011.

(3) Sarshar, M.; Swarctz, C.; Hunter, S.; Simpson, J.; Choi, C. H. Effects of Contact Angle Hysteresis on Ice Adhesion and Growth on Superhydrophobic Surfaces Under Dynamic Flow Conditions. *Colloid Polym. Sci.* **2013**, *291*, 427−435.

(4) Varanasi, K. K.; Deng, T.; Smith, J. D.; Hsu, M.; Bhate, N. Frost Formation and Ice Adhesion on Superhydrophobic Surfaces. *Appl. Phys. Lett.* **2010**, *97*, 234102−3.

(5) Huovinen, E.; Hirvi, J.; Suvanto, M.; Pakkanen, T. A. Micro−Micro Hierarchy Replacing Micro−Nano Hierarchy: A Precisely Controlled Way to Produce Wear-Resistant Superhydrophobic Polymer Surfaces. *Langmuir* **2012**, *28*, 14747−14755.

(6) Xiu, Y.; Liu, Y.; Balu, B.; Hess, D. W.; Wong, C. Robust Superhydrophobic Surfaces Prepared With Epoxy Resin and Silica Nanoparticles. *IEEE Trans. Compon., Packag., Manuf. Technol.* **2012**, *2*, 395−401.

(7) Lacroix, L. M.; Lejeune, M.; Ceriotti, L.; Kormunda, M.; Meziani, T.; Colpo, P.; Rossi, F. Tunable Rough Surfaces: A New Approach for Elaboration of Superhydrophobic Films. *Surf. Sci.* **2005**, *592*, 182−188.

(8) Tian, F.; Hu, A.; Li, M.; Mao, D. Superhydrophobic Nickel Films Fabricated by Electro and Electroless Deposition. *Appl. Surf. Sci.* **2012**, *258*, 3643−3646.

(9) Ma, M.; Mao, Y.; Gupta, M.; Gleason, K. K.; Rutledge, G. C. Superhydrophobic Fabrics Produced by Electrospinning and Chemical Vapor Deposition. *Macromolecules* **2005**, *38*, 9742−9748.

(10) Steele, A.; Bayer, I. S.; Loth, E. Adhesion Strength and Superhydrophobicity of Polyurethane/Organoclay Nanocomposite Coatings. *J. Appl. Polym. Sci.* **2012**, *125*, E445−E452.

(11) Jung, S.; Dorrestijn, M.; Raps, D.; Das, A.; Megaridis, C. M.; Poulikakos, D. Are Superhydrophobic Surfaces Best for Icephobicity? *Langmuir* **2011**, *27*, 3059−3066.

(12) Nosonovsky, M.; Bhushan, B. Hierarchical Roughness Optimization for Biomimetic Superhydrophobic Surfaces. *Ultramicroscopy* **2007**, *107*, 969−979.

(13) Yeong, Y. H.; Davis, A.; Steele, A.; Loth, E.; Bayer, I. S. Spray Deposition Effects on Superhydrophobicity and Durability of Nano-Coatings. *Surf. Innovations* **2014**, *2*, 70−78.

(14) Steele, A.; Bayer, I. S.; Loth, E. Inherently Superoleophobic Nanocomposite Coatings by Spray Atomization. *Nano Lett.* **2009**, *9*, 501−505.

(15) Kulinich, S. A.; Farzaneh, M. How Wetting Hysteresis Influences Ice Adhesion Strength on Superhydrophobic Surfaces. *Langmuir* **2009**, *25*, 8854−8856.

(16) Rasigni, M.; Rasigni, G. Surface Structure Autocorrelation Functions and their Fourier Transforms for Rough Deposits of Magnesium. *Phys. Rev. B: Condens. Matter Mater. Phys.* **1979**, *19*, 1915−1919.

(17) Zhang, Y.; Sundararajan, S. The Effect of Autocorrelation Length on the Real Area of Contact and Friction Behavior of Rough Surfaces. *J. Appl. Phys.* **2005**, *97*, 103526−103532.

(18) Wang, Y.; Xue, J.; Wang, Q.; Chen, Q.; Ding, J. Verification of Icephobic/Anti-icing Properties of a Superhydrophobic Surface. *ACS Appl. Mater. Interfaces* **2013**, *5*, 3370−3381.

(19) Boinovich, L. B.; Emelyanenko, A. M.; Ivanov, V. K.; Pashinin, A. S.; Ding, J. Durable Icephobic Coating for Stainless Steel. *ACS Appl. Mater. Interfaces* **2013**, *5*, 2549−2554.

(20) Kulinich, S. A.; Farhadi, S.; Nose, K.; Du, X. W. Superhydrophobic Surfaces: Are They Really Ice-Repellent? *Langmuir* **2011**, *27*, 25−29.

(21) Arianpour, F.; Farzaneh, M.; Kulinich, S. Hydrophobic and Ice-Retarding Properties of Doped Silicone Rubber Coatings. *Appl. Surf. Sci.* **2013**, *265*, 546−552.

(22) Deng, T.; Varanasi, K. K.; Hsu, M.; Bhate, N.; Keimel, C.; Stein, J.; Blohm, M. Nonwetting of Impinging Droplets on Textured Surfaces. *Appl. Phys. Lett.* **2009**, *94*, 133109−133111.